

Last Interglacial peak in mean ocean temperature due to ocean circulation change

Shackleton, S.^{1*}, Baggenstos, D.², Menking, J.A.³, Dyonisius, M.N.⁴, Bereiter, B.^{2,5}, Bauska, T.K.⁶, Rhodes, R.H.⁶, Brook, E.J.³, Petrenko, V.V.⁴, McConnell, J.R.⁷, Kellerhals, T.², Häberli, M.², Schmitt, J.², Fischer, H.², Severinghaus, J.P.¹

¹Scripps Institution of Oceanography, University of California, San Diego, La Jolla CA, USA

²Climate and Environmental Physics, Physics Institute and Oeschger Center for Climate Change Research, University of Bern, Bern, Switzerland

³College of Earth, Ocean, and Atmospheric Sciences, Oregon State University, Corvallis OR, USA

⁴Earth & Environmental Sciences, University of Rochester, Rochester NY, USA

⁵Laboratory for Air Pollution / Environmental Technology, Empa, 8600 Dübendorf, Switzerland

⁶Department of Earth Sciences, University of Cambridge, Cambridge, UK

⁷Division of Hydrologic Sciences, Desert Research Institute, Reno NV, USA

*Corresponding author: Sarah Shackleton, sshackle@ucsd.edu

Abstract

The Last Interglacial (129-116 ka) represents one of the warmest climate intervals of the last 800,000 years and the most recent time when sea level was meters higher than today. However, the timing and magnitude of peak warmth varies between reconstructions, and the relative importance of individual sources contributing to elevated sea level (mass gain versus seawater expansion) during the Last Interglacial remains uncertain. Here we present the first mean ocean temperature record for this interval from noble gas measurements in ice cores and constrain the thermal expansion component of sea level. Mean ocean temperature reaches its maximum value of $1.1 \pm 0.3^\circ\text{C}$ warmer-than-modern at the end of the penultimate deglaciation at 129 ka, resulting in $0.7 \pm 0.3\text{m}$ of elevated sea level, relative to present. However, this maximum in ocean heat content is a transient feature; mean ocean temperature decreases in the first several thousand years of the interglacial and achieves a stable, comparable-to-modern value by ~ 127 ka. The synchronicity of the peak in mean ocean temperature with proxy records of abrupt transitions in oceanic and atmospheric circulation suggests that the mean ocean temperature maximum is related to the accumulation of heat in the ocean interior during the preceding period of reduced overturning circulation.

41 **Introduction**

42 With a heat capacity one thousand times larger than that of the atmosphere, the ocean plays an
43 important role in regulating the rate and magnitude of global temperature change and represents the
44 largest energy reservoir in the climate system¹. Ocean heat uptake and warming contribute directly to
45 increasing sea level through thermal expansion of seawater and may play a role in future sea level rise
46 through enhanced sub-shelf melting and subsequent mass loss from the Antarctic Ice Sheet². To
47 understand the future role of ocean heat uptake, it is instructive to study ocean temperature change
48 during past warm periods in Earth's history.

49 During the Last Interglacial (LIG, 129-116 ka) surface temperatures were warmer than today,
50 but existing reconstructions differ substantially on the timing and magnitude of peak warmth. A global
51 average (land and ocean) surface temperature reconstruction³ from a compilation of seasonal and
52 annual-average temperature records shows a maximum of 2°C warmer temperatures during the middle
53 of the LIG. A global annual-average sea surface temperature (SST) reconstruction⁴ shows a maximum
54 of only 0.5°C warmer-than-preindustrial on a global scale that peaks during the earlier LIG, but up to
55 1°C warmer in the high latitudes. Climate models show considerable warmth at the mid-LIG, especially
56 in the high northern latitudes, but in line with the lack of global insolation forcing, little warming or
57 even cooler conditions on a global scale⁵. At the same time, global sea level during the LIG was 6-9 m
58 higher⁶. Differences in greenhouse gas and orbital forcing over the LIG relative to modern make the
59 spatial and temporal patterns of temperature change during this period distinct from what might be
60 expected from anthropogenic warming⁷. As a result, the LIG is not an analogue for future warming but
61 offers a unique opportunity to assess the validity of earth system model predictions of sea level rise in
62 response to warming, provided that reliable paleoclimate data exist for model validation⁸.

63 Sediment cores provide valuable records of changes in ocean conditions through the LIG^{4,9-11}
64 and are critical to understanding the spatiotemporal structure of temperature change. However, because
65 most available records document surface ocean conditions, deducing total ocean heat content and
66 thermosteric sea level from these records remains challenging.

67 The measurement of atmospheric noble gases trapped in glacial ice provides a method to
68 reconstruct changes in mean ocean temperature (MOT) independently from marine records¹²⁻¹⁴.
69 Changes in the relative atmospheric concentrations of krypton, xenon and nitrogen trace total ocean
70 heat content because they are caused by temperature-driven changes in gas solubilities in seawater.
71 Here, we report measurements of the ratios of Kr/N₂, Xe/N₂, and Xe/Kr in ice cores from Taylor Glacier
72 and EPICA Dome C (EDC) ice cores that cover the LIG and penultimate glacial, Marine Isotope Stage
73 6 (MIS6, 180-136 ka). We assess the timing and magnitude of ocean temperature change during the
74 LIG and quantify the thermosteric component of elevated sea level during this period.

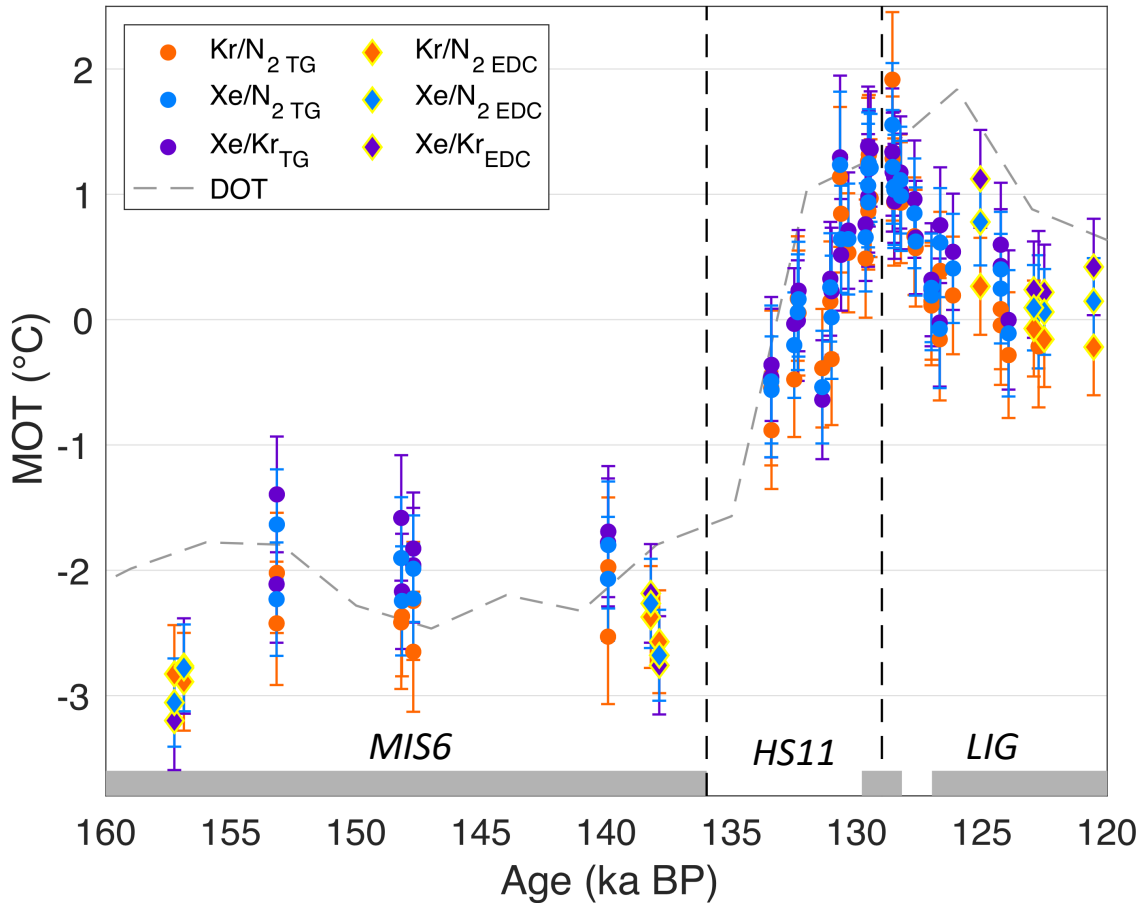
75

76 **Last Interglacial mean ocean temperature record**

77 MOT anomalies are calculated relative to the Early Holocene (11– 10 ka) for each ice core
78 because firn fractionation corrections are more robust when calculating relative MOT change
79 compared to absolute MOT values (supplement). MOT anomalies relative to the preindustrial and
80 modern are subsequently calculated using the existing WAIS Divide¹² and EDC¹⁵ Holocene-to-
81 preindustrial MOT records and preindustrial-to-modern simulations of ocean temperature change¹⁶.
82 Based on Monte Carlo simulations that account for all known sources of uncertainty (methods), we
83 constrain peak MOT to $1.1\pm 0.3^{\circ}\text{C}$ (1σ) warmer than modern at 129.0 ± 0.8 ka on the Antarctic Ice
84 Core Chronology (AICC2012)¹⁷ (Figure 1). While data for MIS6 and Termination II are relatively
85 sparse, the period of maximum MOT is highly resolved (methods). Because of this and the robust
86 age constraints from trace gas measurements for the Taylor Glacier record (methods/supplement),
87 the timing of peak MOT is well constrained.

88 The record shows a $3.4\pm 0.5^{\circ}\text{C}$ MOT increase from MIS6 to the early LIG, compared to the
89 LGM to Holocene change of $2.6\pm 0.3^{\circ}\text{C}$ ¹². The larger magnitude in glacial-interglacial MOT change
90 over Termination II versus Termination I is consistent with previous reconstructions of deep ocean
91 temperature during these intervals from stacks of low-resolution marine records¹¹.

92



93

94 **Figure 1. Mean Ocean Temperature (MOT) anomaly from Kr/N₂, Xe/N₂, and Xe/Kr.** MOT
 95 data is shown with 1 σ error (methods). Vertical dashed lines mark the Marine Isotope Stage 6
 96 (MIS6), Heinrich Stadial 11 (HS11) and Last Interglacial (LIG) boundaries. Gray bars indicate the
 97 time intervals for which MIS6 MOT (>136 ka), peak MOT (129.0 \pm 0.8 ka), and stable LIG MOT
 98 (<127 ka) are calculated. MOT is reported on the AICC2012¹⁷ chronology. Global average deep
 99 ocean temperature (DOT) from stacked marine sediment records¹¹ on LR04¹⁸ is shown for
 100 reference.

101

102

103 Comparison to global surface temperature records

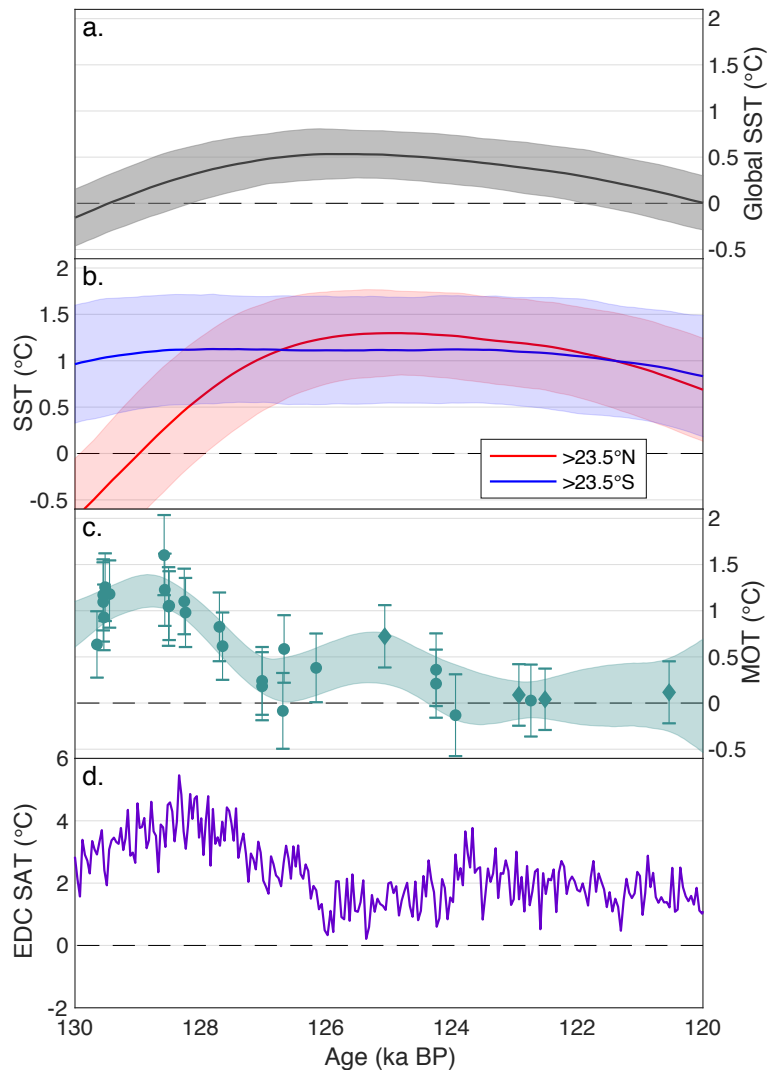
104

105 Comparison of our MOT record to stacked SST records from marine sediments⁴ over the
 106 LIG reveal distinct differences between these fundamental climate parameters (Figure 2). The
 107 maximum in MOT occurs earlier and exceeds the magnitude of the global SST maximum. The
 108 magnitude of the peak extratropical SST anomaly agrees well with the peak MOT anomaly, though
 109 the temporal evolution of each record over the LIG appears distinct. Comparison of the timing of
 110 MOT and SST change is complicated by the lack of absolute age constraints for sediment and ice
 111 core records spanning the LIG, and a 1-2 thousand year offset between the SpeleoAge¹⁹ and
 AICC2012 chronologies that are applied to the SST and MOT records respectively²⁰. However,

112 accounting for the offset in chronologies would actually increase the offset in the relative timing of
113 the MOT and global SST maxima.

114 While global SST records are good indicators of the ‘skin temperature’ and thus outgoing
115 longwave radiation for much of the planet, MOT is closely related to subsurface heat content¹⁵.
116 MOT represents volume-averaged ocean temperature, so changes in intermediate and deep ocean
117 temperatures (as opposed to SST changes) play a dominant role in setting MOT. Much of the
118 intermediate and deep ocean’s temperature is set at high latitudes via meridional circulation, so the
119 polar regions are likely crucial for the structure of MOT change, relative to that of global SST²¹.

120 MOT and Antarctic surface temperature²² records show strikingly similar features (Figures
121 2 and 3). Both records are reported on AICC2012, but minor uncertainties in their alignment may
122 result from error in the Taylor Glacier chronology, or the EDC gas-ice age difference²³. The
123 covariation of MOT and Antarctic temperature during the LIG follows the pattern recently observed
124 during Termination I^{12,15} in which mean ocean and high southern latitude surface warming precede
125 the increase in global SST and appear intrinsically linked. We thus have strong evidence that
126 changes in MOT outpace and exceed low latitude SST changes during the LIG, which suggest that
127 polar amplification and intermediate/deep-water formation are key regulators of MOT.



128

129 **Figure 2. Surface and mean ocean temperature (MOT) anomalies during the LIG.** a) global
 130 and b) extratropical sea surface temperatures (SST) (relative to preindustrial) from the Northern
 131 Hemisphere (red) and Southern Hemisphere (blue) from stacked SST proxy records⁴ on the
 132 SpeleoAge chronology¹⁹. Shading shows 2 σ confidence interval. c) MOT (relative to modern) on
 133 AICC2012¹⁷ with 1 σ error bars (points) and 1 σ confidence envelope (shading). d) EPICA Dome C
 134 (EDC) surface air temperature²² (SAT, relative to average of last 1000 years) on AICC2012.
 135

136 **Links of MOT and ocean circulation over Termination II/LIG**

137 Recent studies have investigated the role of the bipolar seesaw, the out-of-phase
 138 temperature variations between hemispheres, in the evolution of glacial terminations^{10,19,24,25}. While
 139 the exact triggering mechanisms are still debated, it is generally accepted that the bipolar pattern
 140 of global temperature anomalies is the result of variations in the strength of the Atlantic Meridional
 141 Overturning Circulation (AMOC)²⁶. When AMOC is in a strong mode, as today, there is northward

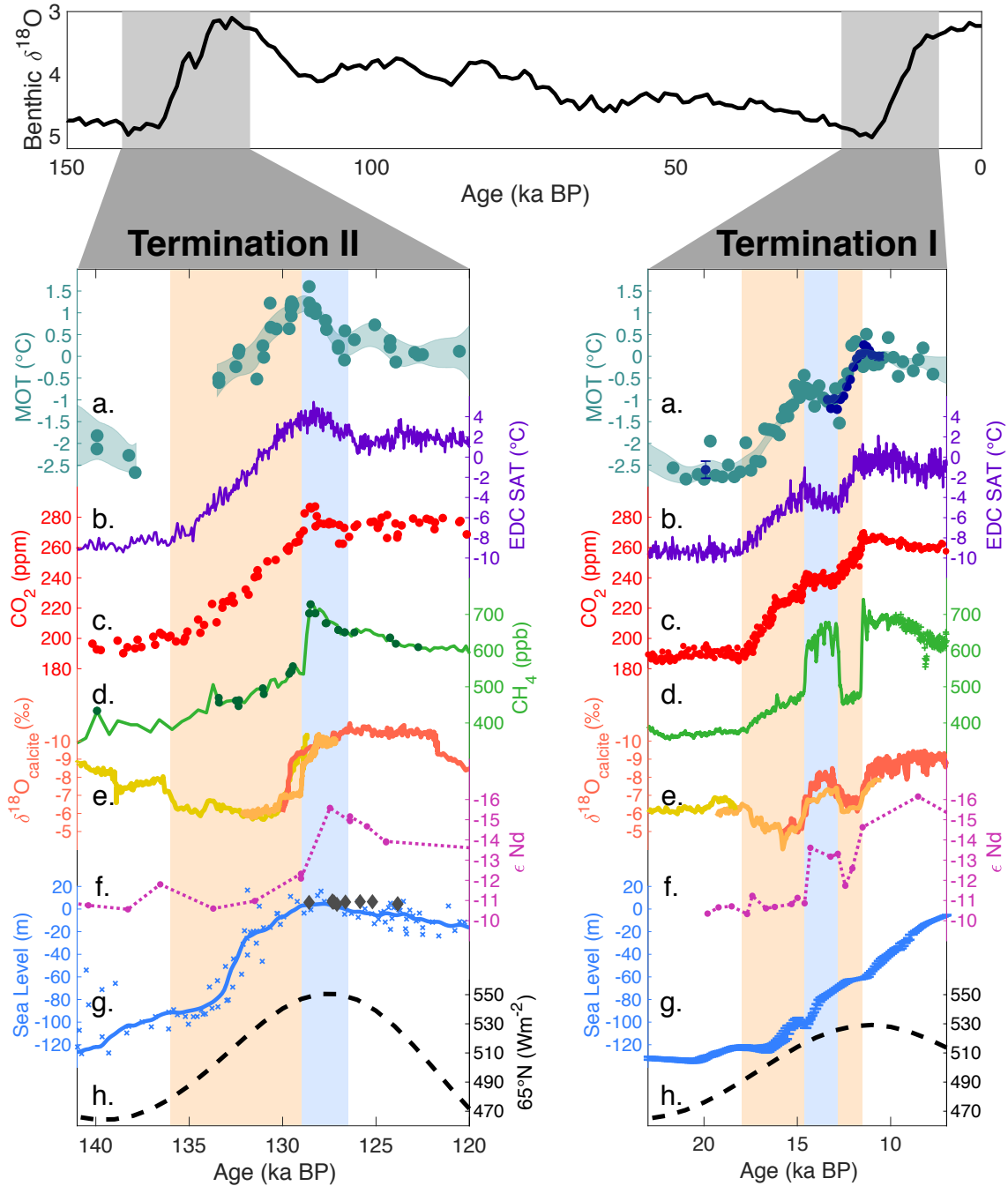
142 heat transport at all latitudes in the Atlantic. When AMOC is weakened, this heat transport is
143 reduced, leading to a net accumulation of heat in the Southern Hemisphere.

144 A recent synthesis of available high-resolution records covering Termination II²⁷ including
145 sediment records from the North Atlantic¹⁰, Chinese speleothems²⁵, and Antarctic ice cores^{28,29}
146 suggest that the AMOC was considerably weakened during Heinrich Stadial 11 (HS11, ~136-129
147 ka), a cold period in the Northern Hemisphere that covers much of Termination II. At ~129 ka,
148 these proxy records show a rapid recovery of AMOC and Asian monsoon strength, coinciding with
149 an abrupt shift in Antarctic moisture source²⁸, CH₄ increase²⁹, and the peak in MOT in our
150 reconstruction (Figure 3). Because CH₄ and noble gases are measured on the same ice samples,
151 there is virtually no uncertainty in the relative timing of the abrupt rise in CH₄ and the MOT
152 maximum (supplement). The excellent agreement in the timing of peak MOT (129.0±1.9 ka,
153 including AICC2012 uncertainty) and the end of HS11 (128.9±0.06 ka) dated from the Sanbao
154 Cave records²⁵ also suggests an important connection between MOT and the bipolar seesaw.

155 Recent modeling studies have examined the impact of reduced AMOC on surface and
156 subsurface temperature change through freshwater hosing experiments^{14,26,30}. In these simulations,
157 reduction in AMOC strength results in a globally asymmetric surface pattern of cold Northern
158 Hemisphere SSTs, as Southern Hemisphere SSTs, MOT, and Antarctica temperatures increase. At
159 the subsequent recovery of the AMOC, the accumulated subsurface heat is released, leading to an
160 abrupt increase in Northern Hemisphere SST, and gradual decrease in Southern Hemisphere SST,
161 Antarctic temperature, and MOT²⁶. This spatiotemporal pattern is consistent with the observed
162 Antarctic temperature and MOT trends during HS11 and the LIG (Figure 3). As in the hosing
163 simulations, we observe MOT and Antarctic temperature increase during the weakened AMOC
164 interval of HS11, reach a maximum at ~129 ka synchronous with AMOC recovery¹⁰, and then
165 decrease during the several thousand years following AMOC recovery. This mechanism is also
166 consistent with the lead of Southern Hemisphere over Northern Hemisphere high latitude warming
167 that is observed at the onset of the LIG^{4,9}.

168 These observations raise the question³¹ of how much of the warmer-than-modern MOT in
169 the early LIG was due to the weakened AMOC state, and how much can be attributed to the stable
170 interglacial climate. In our record, MOT decreased and eventually stabilized by ~127 ka (at latest
171 by ~124 ka) at a temperature that is comparable to Holocene/modern MOT (+0.2±0.3°C). If the
172 observed MOT decrease was due to the release of stored heat post-AMOC recovery, then we can
173 attribute most of the MOT anomaly at the LIG onset to deglacial changes in ocean circulation.

174



175

176 **Figure 3. Climate records of Terminations II and I.** Left panel: climate records of Termination
 177 II. **a)** Mean ocean temperature (MOT) anomaly relative to modern from this study with 1σ error
 178 (shading). **b)** Antarctic temperature²² anomaly relative to average of last 1000 years, **c)** CO_2 ³², and
 179 **d)** CH_4 ²⁹. Green points show Taylor Glacier CH_4 measurements. **a)-d)** are presented on AICC2012¹⁷.
 180 **e)** Sanbao^{25,33} ^{230}Th -dated $\delta^{18}\text{O}_{\text{calcite}}$ records. Colors distinguish individual speleothems. **f)** North
 181 Atlantic ϵNd^{10} on core-specific age scale. **g)** Red Sea Level anomaly corrected for isostatic effects³⁴
 182 on core-specific age scale (light blue). Gray diamonds show coral reef sea level records³⁵. **h)**
 183 Summer solstice insolation at 65°N . Right panel: climate records of Termination I with differences

184 from left panel as follows. **a**) MOT anomaly relative to modern from WAIS Divide¹² (turquoise)
185 and Taylor Glacier³⁶ (dark blue). Error bars show spread (1σ) of replicate samples measured at SIO
186 for this study (supplement). **c**) CO₂³⁷, and **d**) CH₄³⁸. **a**), **c**) and **d**) are presented on WD2014³⁹. **e**)
187 Dongge⁴⁰ (red) and Hulu⁴¹ (orange and yellow) $\delta^{18}\text{O}_{\text{calcite}}$ records. **f**) North Atlantic ϵNd^{42} on core-
188 specific age scale **g**) eustatic sea level⁴³ with 1σ error from radiocarbon/uranium-series dated coral
189 and sediment records. Orange bars indicate times when AMOC was in a weakened mode and blue
190 bars show periods of strong AMOC and mean ocean/Antarctic cooling. Top panel: benthic $\delta^{18}\text{O}$ on
191 LR04¹⁸. Gray bars highlight the intervals shown in the panels below.
192

193 While our Termination II record of MOT lacks resolution at its onset, the only observed
194 warming occurs during the weakened AMOC interval, HS11. Northern Hemisphere insolation
195 forcing during Termination II exceeded that of Termination I, which may in part explain the
196 comparatively rapid disintegration of the Northern Hemisphere ice sheets during Termination II,
197 and long duration of suppressed AMOC due to strong freshwater forcing of the North Atlantic²⁴.
198 During Termination I the AMOC temporarily recovered, possibly due to the weaker insolation and
199 thus reduced freshwater forcing⁴⁴. During this time, both Antarctic temperatures and MOT
200 decreased (Figure 3). The so-called ‘Antarctic Cold Reversal’, may in many ways be analogous to
201 the Antarctic and mean ocean cooling observed at the end of Termination II, post-AMOC recovery.
202 While the magnitude of MOT decrease over the Antarctic Cold Reversal was slightly smaller than
203 what is observed for the LIG onset, the net mean ocean warming during Heinrich Stadial I¹² and
204 the Younger Dryas³⁶ of $3.4\pm 0.4^\circ\text{C}$ is remarkably similar to the net warming found from MIS6 to
205 the LIG peak observed in our record ($3.4\pm 0.5^\circ\text{C}$). In addition, the magnitude of glacial-interglacial
206 change across Termination II once MOT has stabilized is $2.5\pm 0.5^\circ\text{C}$, which is comparable to the
207 magnitude of MOT change across Termination I ($2.6\pm 0.3^\circ\text{C}$). Several studies comparing
208 Terminations I and II have posited that the larger magnitude of changes in Antarctic temperature²⁸
209 and CO₂¹⁰ across Termination II are related to the delayed recovery of AMOC strength. Our record
210 suggests the same is true for MOT.

211 These observations suggest that the AMOC interruptions during the past two terminations
212 transiently provided an additional $\sim 1^\circ\text{C}$ of mean ocean warming above the net glacial-interglacial
213 MOT change. A recent quantitative assessment of Earth’s radiative imbalance over Termination I¹⁵
214 found maxima in positive radiative imbalance during the Younger Dryas and Heinrich Stadial I,
215 suggesting that reduced AMOC during these intervals contributed energy to the climate system
216 through an increase in ocean heat storage. This storage and subsequent release of energy may play
217 a critical role in terminations³⁰. As shown in simulations³⁰, when the AMOC is reduced the
218 subsurface ocean works as a ‘capacitor’, storing heat while the surface (centered on the North
219 Atlantic) remains cold. Once the AMOC recovers, the subsurface heat is released, providing

220 enhanced surface warming. While our MOT record lacks the necessary resolution to conduct a
221 similar assessment of radiative imbalance across Termination II, the comparable magnitudes of
222 enhanced mean ocean warming during weakened AMOC intervals over the last two terminations
223 suggest that this mechanism was also important for Termination II. Along with the potential
224 importance of AMOC interruptions in releasing Southern Ocean CO₂^{45,46} and destabilizing Northern
225 Hemisphere ice sheets^{47,48}, their role in providing additional energy to the climate system lends
226 support to the hypothesis that AMOC interruptions are not merely incidental to terminations, but
227 play a role in driving the climate out of glacial conditions^{19,25}.

228

229 **Implications for West Antarctic Ice Sheet stability**

230 The MOT changes across the LIG have direct and indirect implications for sea level.
231 Pinning down the sources contributing to the LIG global mean sea level highstand is crucial to
232 understand the vulnerability of modern ice sheets to global warming. From CMIP5 estimates of the
233 expansion efficiency of heat (0.12 m YJ⁻¹)⁴⁹, we find that the 1.1±0.3°C MOT anomaly during the
234 early stages of the LIG contributed 0.7±0.3m to elevated sea level. By ~127 ka MOT had decreased
235 to near-modern values, and no appreciable thermosteric contribution (relative to modern) is
236 expected by this early stage in the interglacial. In fact, our record implies a trend of thermosteric
237 sea level lowering in the first several thousand years of the LIG. Coral reef records indicate that
238 sea level was already 5.9±1.7m higher than modern at 128.6±0.8ka³⁵, requiring a substantial ice
239 sheet (in addition to the thermosteric) contribution early in the LIG to explain this magnitude of
240 elevated sea level.

241 The early maximum in MOT may have played another, more indirect role in contributing
242 to sea level rise during the LIG. In recent Antarctic Ice Sheet simulations of the LIG^{50,51}, ocean
243 warming played an important role in mass loss from the West Antarctic Ice Sheet. Ref. 50 found
244 that if ocean warming occurred shortly after the glacial termination, the West Antarctic Ice Sheet
245 was more prone to lose mass because of enhanced reverse-sloped beds at grounding lines. By
246 invoking sub-shelf melting through Southern Ocean warming, ref. 51 derived the highest rates of
247 sea level rise during maximum Antarctic temperatures at the end of Termination II, synchronous to
248 our MOT maximum. The delay in AMOC recovery and resulting accumulation of heat in the ocean
249 interior and Southern Hemisphere at the end of Termination II may therefore have played an
250 important role in West Antarctic Ice Sheet mass loss and elevated sea level during the LIG.

251 An important caveat to consider for this hypothesis is that MOT is not a proxy for ocean
252 temperatures directly under ice shelves, and higher MOT does not necessarily imply that
253 temperatures in vulnerable sub-ice shelf regions were enhanced. However, MOT and the

254 temperature of circumpolar deep water are intrinsically linked because circumpolar deep water is
255 made up of a representative mixture of waters from all ocean basins⁵² and is brought efficiently to
256 the surface by isopycnal mixing in the Southern Ocean. If, as today, circumpolar deep water
257 intruded onto the Antarctic continental shelf, its ice melting capacity would be enhanced during the
258 early stages of the LIG.

259

260 **Conclusions**

261 The ocean heat anomaly provided from our MOT reconstruction is a simple but important
262 metric to evaluate in earth system models, making it useful for forthcoming simulations of the LIG.
263 Comparison with other proxy and model results suggest that peak MOT coincided with the abrupt
264 recovery of the AMOC at the end of Termination II and was a transient rather than stable feature
265 of the LIG. Enhanced MOT contributed to elevated thermohaline sea level during the early stages
266 of the LIG and may have played a more indirect role in the sea level highstand through amplified
267 melting of ice sheets and shelves from below. The temporal evolution of AMOC and MOT over
268 the past two terminations suggest that the ocean's overturning circulation plays a dominant role in
269 controlling the timing and magnitude of MOT change across terminations; studying the LIG in the
270 context of the termination that preceded it provides a more complete view of the climate evolution
271 that occurred over this interval.

272

273 **Methods**

274

275 **Taylor Glacier sampling and site description**

276

277 Taylor Glacier is an outlet glacier of the East Antarctic Ice Sheet with a >80 km long
278 ablation zone exposing easily accessible old ice at the surface. Its accumulation zone is located on
279 the northern flank of Taylor Dome and it terminates in Taylor Valley. Extensive work on mapping
280 the stratigraphy of the glacier identified ice from the LIG located near the terminus of the glacier<sup>53-
281 55</sup>.

282 For this study, a total of four large-diameter ice cores were collected during the 2014/15
283 and 2015/16 Antarctic field seasons (Figure S1 in supplement). Two cores spanning approximately
284 155 – 120 ka were collected approximately 4 km from the glacier terminus. Additionally, two cores
285 were drilled along a previously-established across-flow transect⁵³ from the early Holocene (10.6
286 ka) and Last Glacial Maximum (LGM, 19.9 ka) to serve as a comparison to LIG and MIS6 MOT
287 samples. Cores were drilled with the Blue Ice Drill⁵⁶ and are 24.1 cm in diameter. Cores were
288 processed and subdivided in the field and analyzed for noble gases for MOT reconstruction as well
289 as other atmospheric gases used to establish the chronology of the record.

290

291 **Taylor Glacier core chronology**

292

293 A major challenge in sampling a blue ice area is establishing ages for the samples⁵⁷. Ice
294 from Taylor Glacier has traveled tens of kilometers from its deposition site and has likely
295 undergone non-uniform thinning and folding. While the dynamics of the glacier have been studied

296 in detail^{58,59}, not enough is known about the basal topography or subsurface ice flow to build a
297 chronology for the glacier from a glaciological model.

298 We therefore use alternative methods to construct the chronology for our samples. Previous
299 work in blue ice areas^{53,60–62} has demonstrated success in establishing ice sample chronologies
300 through value and/or inflection point matching of well-mixed atmospheric gases to well-dated ice
301 core records⁶³. For this study the chronology was constructed using a least-squares fitting method
302 with measurements of methane concentrations (CH₄), molecular oxygen isotopic composition
303 ($\delta^{18}\text{O}_{\text{atm}}$), and carbon dioxide concentrations (CO₂), tied to EPICA Dome C (EDC) reference
304 records^{29,32,64} on the Antarctic Ice Core Chronology (AICC2012)^{17,65}. This method allows for a
305 construction of an age probability distribution for each noble gas sample that can be used to assess
306 sample age uncertainty (supplement).

307

308 **Taylor Glacier noble gas measurements**

309

310 Taylor Glacier measurements of noble gases for MOT reconstruction were made at Scripps
311 Institution of Oceanography (SIO). A total of 45 ice samples from the 2014/15 and 2015/16 cores
312 were analyzed, including eight replicate samples, giving 37 unique MOT samples. Of the 45
313 samples, 3 were rejected due to sample age uncertainty (see supplement). In addition, at SIO and
314 Bern five samples from the Holocene (10.6 ka) and five from the LGM (19.9 ka) were measured
315 (Figure 3) at each institution. The motivation for this analysis was to verify the quality of the noble
316 gas records by comparison to published MOT records¹², and to verify that any offsets in the EDC
317 and Taylor Glacier MOT results were unrelated to lab offsets (see supplementary materials).

318 The analytical methods for noble gas measurements are described in detail by Bereiter et
319 al. (2018b). In short, ~800 grams of ice were melted under vacuum and liberated gases (~80 ml at
320 standard temperature and pressure, STP) were cryogenically trapped in stainless steel dip tubes.
321 After gas extraction, the samples were split into two aliquots. The larger (~78 ml STP) aliquot was
322 exposed to a Zr/Al alloy at 900°C to remove all non-noble gases and measured on a Thermo-
323 Finnigan MAT-253 isotope ratio mass spectrometer via dual inlet method for ⁴⁰Ar/³⁸Ar ($\delta^{40/38}\text{Ar}$),
324 ⁴⁰Ar/³⁶Ar ($\delta^{40/36}\text{Ar}$), ⁸⁶Kr/⁸⁴Kr ($\delta^{86/84}\text{Kr}$), ⁸⁶Kr/⁸³Kr ($\delta^{86/83}\text{Kr}$), ⁸⁶Kr/⁸²Kr ($\delta^{86/82}\text{Kr}$), ⁸⁴Kr/⁴⁰Ar ($\delta\text{Kr}/\text{Ar}$),
325 and ¹³²Xe/⁴⁰Ar ($\delta\text{Xe}/\text{Ar}$). The smaller aliquot (~2 ml, STP) was passed through a cryotrap (-196°C)
326 to remove CO₂ and measured on a Thermo-Finnigan MAT Delta V isotope ratio mass spectrometer
327 via dual inlet method for ²⁹N₂/²⁸N₂ ($\delta^{15}\text{N}$), ³⁴O₂/³²O₂ ($\delta^{18}\text{O}$), ³²O₂/²⁸N₂ ($\delta\text{O}_2/\text{N}_2$), and ⁴⁰Ar/²⁸N₂
328 ($\delta\text{Ar}/\text{N}_2$). Measurements were corrected for pressure imbalance and chemical slope according to
329 established procedure⁶⁷.

330 All data are reported in delta notation, relative to a modern atmosphere standard. Because
331 argon is preferentially lost relative to xenon and krypton during ice bubble formation⁶⁸, we
332 mathematically combine $\delta\text{Xe}/\text{Ar}$, $\delta\text{Kr}/\text{Ar}$, and $\delta\text{Ar}/\text{N}_2$ to obtain $\delta\text{Kr}/\text{N}_2$, $\delta\text{Xe}/\text{N}_2$, and $\delta\text{Xe}/\text{Kr}$.

333

334 **Taylor Glacier fractionation corrections**

335

336 To reconstruct ocean temperature from Kr/N₂, Xe/N₂ and Xe/Kr, it is necessary to correct
337 for fractionation during firnification, the process by which fresh snow compacts, transitioning to
338 denser firn and eventually to glacial ice containing air trapped in bubbles. While the free
339 troposphere is well mixed through convective processes, the low permeability of the firn restricts
340 bulk flow; gases within the firn column are transported primarily via molecular diffusion⁶⁹. This
341 allows for gravitational settling and thermal diffusion to alter firn air from its atmospheric
342 composition before it is occluded in glacial ice^{70,71}. As such, Kr/N₂, Xe/N₂ and Xe/Kr must be
343 corrected for fractionating processes to derive the paleoatmospheric composition for inferring
344 MOT.

345 As suggested by ref. 12, under/over-correction of fractionation may lead to systematic
346 offsets in MOT, but the effect primarily impacts the absolute MOT anomaly (relative to modern)
347 and has little impact on relative MOT change within a record. We investigate the influence of the
348 choice in methods of fractionation correction on the MOT record and find that different methods
349 shift the absolute MOT record up or down but have little effect on relative MOT change in the
350 Taylor Glacier record (see supplement). We thus compute the MOT anomalies relative to the Taylor
351 Glacier Holocene (10.6 ka) samples and then estimate the Holocene – modern MOT difference
352 (and uncertainties) from the WAIS Divide MOT record and model simulations of ocean heat
353 content over the last 2000 years¹⁶. A detailed description and assessment of the fractionation
354 corrections is included in the supplementary materials.

355 **EDC ice core noble gas analysis**

356 Four EDC ice core samples from the LIG and four from MIS6 were analyzed at the
357 University of Bern and included in this study. Measurement and data processing for these samples
358 are similar to the analysis of Taylor Glacier samples with a few important distinctions (ref. 15 and
359 supplement). Chronological uncertainties are not considered in this analysis, because the Taylor
360 Glacier chronology is tied to that of EDC through ice core synchronization and contribute
361 minimally to the total uncertainty for these samples. In addition, the approach to firn fractionation
362 corrections differs slightly between Taylor Glacier and EDC (supplementary section SI4).

363 **Derivation of MOT from noble gas data**

364 To reconstruct MOT values from fractionation-corrected Kr/N₂, Xe/N₂ and Xe/Kr, we use
365 the ocean-atmosphere box model of ref. 12 with several modifications. We make no assumptions
366 about the glacial-interglacial change in the ocean saturation state and use current estimates of
367 krypton and xenon undersaturation⁷² in the box model for the entirety of the record. We also do not
368 invoke the glacial-interglacial changes in the relative water mass distributions that were applied in
369 ref. 12 and use the modern distributions of Antarctic Bottom Water and North Atlantic Deep Water
370 to derive MOT over the full record.

371 We account for the effects of changes in ocean salinity, volume, and atmospheric pressure
372 on the oceanic inventories of krypton, xenon and nitrogen using the sea level record of ref. 34
373 corrected for isostatic effects (supplement). We also include the influence of the large ice shelf over
374 the Arctic during MIS6, which holds the equivalent of 15 meters of sea level, influencing ocean
375 salinity and volume, but not sea level⁷³.

376 To assess uncertainty in our MOT record we run 10,000 Monte Carlo simulations of our
377 reconstruction with all known analytical and dating uncertainties in the MOT and sea level records,
378 as well as the uncertainty in the Holocene-to-modern MOT change. We include uncertainties in
379 measured Kr/N₂, Xe/N₂ and Xe/Kr and the isotope data used to correct for firn processes in our
380 simulations, as well as the method used for fractionation corrections (supplementary section SI4).
381 To account for age uncertainties in the MOT record, we use an inverse transform method⁷⁴ to
382 randomly sample from our age probability distribution to include in our Monte Carlo simulations.
383 For our final uncertainty estimate, we use the average of the three MOT records (and the Monte
384 Carlo simulations) from Kr/N₂, Xe/N₂ and Xe/Kr to minimize the influence of analytical noise from
385 any single measurement.

386 The 1 σ confidence envelope shown in Figures 2 and 3 was constructed using the MATLAB
387 cubic smoothing spline function (csaps) with a 2500 year cut off period on the 10,000 Monte Carlo
388 MOT reconstructions. Each reconstruction was resampled using a bootstrapping method before the
389 spline was produced. The 1 σ confidence envelope was then calculated from the distribution of the
390 Monte Carlo splines at each time interval in the record.

391

396 **Data availability**

397 Presented data are available online at (*****).

398

399 **References**

- 400 1. Stocker, T. F. *et al.* Climate change 2013: The physical science basis. (2013).
- 401 2. Pritchard, H. D. *et al.* Antarctic ice-sheet loss driven by basal melting of ice shelves.
402 *Nature* **484**, 502–505 (2012).
- 403 3. Snyder, C. W. Evolution of global temperature over the past two million years. *Nature*
404 **538**, 226–228 (2016).
- 405 4. Hoffman, J. S., Parnell, A. C. & He, F. Regional and global sea-surface temperatures
406 during the last interglaciation. *Science* **279**, 276–279 (2017).
- 407 5. Otto-Bliesner, B. L. *et al.* How warm was the last interglacial? New model – data
408 comparisons. *Philos. Trans. R. Soc. A* **371**, (2013).
- 409 6. Kopp, R. E., Simons, F. J., Mitrovica, J. X., Maloof, A. C. & Oppenheimer, M.
410 Probabilistic assessment of sea level during the last interglacial stage. *Nature* **462**, 863–
411 867 (2009).
- 412 7. Masson-Delmotte, V. *et al.* Sensitivity of interglacial Greenland temperature and
413 $\delta^{18}\text{O}$: ice core data, orbital and increased CO_2 climate simulations. *Clim. Past* **7**,
414 1041–1059 (2011).
- 415 8. Fischer, H. *et al.* Palaeoclimate constraints on the impact of 2°C anthropogenic warming
416 and beyond. *Nat. Geosci.* **11**, 475–485 (2018).
- 417 9. Capron, E. *et al.* Temporal and spatial structure of multi-millennial temperature changes at
418 high latitudes during the Last Interglacial. *Quat. Sci. Rev.* **103**, 116–133 (2014).
- 419 10. Deaney, E. L., Barker, S. & Flierdt, T. Van De. Timing and nature of AMOC recovery
420 across Termination 2 and magnitude of deglacial CO_2 change. *Nat. Commun.* **8**, 1–10
421 (2017).
- 422 11. Shakun, J. D., Lea, D. W., Lisiecki, L. E. & Raymo, M. E. An 800-kyr record of global
423 surface ocean $\delta^{18}\text{O}$ and implications for ice volume-temperature coupling. *Earth Planet.*
424 *Sci. Lett.* **426**, 58–68 (2015).
- 425 12. Bereiter, B., Shackleton, S., Baggenstos, D., Kawamura, K. & Severinghaus, J. Mean
426 global ocean temperatures during the last glacial transition. *Nature* **553**, 39–44 (2018).
- 427 13. Headly, M. A. & Severinghaus, J. P. A method to measure Kr/N_2 ratios in air bubbles
428 trapped in ice cores and its application in reconstructing past mean ocean temperature. *J.*
429 *Geophys. Res.* **112**, 1–12 (2007).
- 430 14. Ritz, S. P., Stocker, T. F. & Severinghaus, J. P. Noble gases as proxies of mean ocean
431 temperature : sensitivity studies using a climate model of reduced complexity. *Quat. Sci.*
432 *Rev.* **30**, 3728–3741 (2011).
- 433 15. Baggenstos, D. *et al.* The Earth’s radiative imbalance from the Last Glacial Maximum to
434 the present. *Proc. Natl. Acad. Sci.* **116**, 14881–14886 (2019).
- 435 16. Gebbie, G. & Huybers, P. The Little Ice Age and 20th-century deep Pacific cooling.
436 *Science* **363**, 70–74 (2019).
- 437 17. Bazin, L. *et al.* An optimized multi-proxy, multi-site Antarctic ice and gas orbital
438 chronology (AICC2012): 120-800 ka. *Clim. Past* **9**, 1715–1731 (2013).
- 439 18. Lisiecki, L. E. & Raymo, M. E. A Pliocene-Pleistocene stack of 57 globally distributed
440 benthic $\delta^{18}\text{O}$ records. *Paleoceanography* **20**, (2005).
- 441 19. Barker, S. *et al.* 800,000 Years of Abrupt Climate Variability. *Science* **334**, 347–352
442 (2011).
- 443 20. Capron, E., Govin, A., Feng, R., Otto-Bliesner, B. L. & Wolff, E. W. Critical evaluation
444 of climate syntheses to benchmark CMIP6 / PMIP4 127 ka Last Interglacial simulations in

- 445 the high-latitude regions. *Quat. Sci. Rev.* **168**, 137–150 (2017).
- 446 21. Gebbie, G. & Huybers, P. How is the ocean filled? *Geophys. Res. Lett.* **38**, (2011).
- 447 22. Jouzel, J. *et al.* Orbital and Millennial Antarctic Climate Variability over the Past 800,000
448 years. *Science* **317**, 793–796 (2007).
- 449 23. Parrenin, F. *et al.* On the gas-ice depth difference (Δ depth) along the EPICA Dome C ice
450 core. *Clim. Past* **8**, 1239–1255 (2012).
- 451 24. Marino, G. *et al.* Bipolar seesaw control on last interglacial sea level. *Nature* **522**, 197–
452 201 (2015).
- 453 25. Cheng, H. *et al.* Ice Age Terminations. *Science* **326**, 248–252 (2009).
- 454 26. Pedro, J. B. *et al.* Beyond the bipolar seesaw: Toward a process understanding of
455 interhemispheric coupling. *Quat. Sci. Rev.* **192**, 27–46 (2018).
- 456 27. Menviel, L. *et al.* The penultimate deglaciation: protocol for PMIP4 transient numerical
457 simulations between 140 and 127 ka, version 1.0. *Geosci. Model Dev. Discuss.* (2019).
- 458 28. Masson-Delmotte, V. *et al.* Abrupt change of Antarctic moisture origin at the end of
459 Termination II. *Proc. Natl. Acad. Sci.* **107**, 10–13 (2010).
- 460 29. Louergue, L. *et al.* Orbital and millennial-scale features of atmospheric CH₄ over the past
461 800,000 years. *Nature* **453**, 383–386 (2008).
- 462 30. Galbraith, E. D., Merlis, T. M. & Palter, J. B. Destabilization of glacial climate by the
463 radiative impact of Atlantic Meridional Overturning Circulation disruptions. *Geophys.*
464 *Res. Lett.* **43**, 8214–8221 (2016).
- 465 31. Barker, S. *et al.* Early interglacial legacy of deglacial climate instability. *Paleoceanogr.*
466 *Paleoclimatology* (2019). doi:10.1029/2019PA003661
- 467 32. Schneider, R., Schmitt, J., Köhler, P., Joos, F. & Fischer, H. A reconstruction of
468 atmospheric carbon dioxide and its stable carbon isotopic composition from the
469 penultimate glacial maximum to the last glacial inception. *Clim. Past* **9**, 2507–2523
470 (2013).
- 471 33. Wang, Y. *et al.* Millennial- and orbital-scale changes in the East Asian monsoon over the
472 past 224,000 years. *Nature* **451**, 1090–1093 (2008).
- 473 34. Grant, K. M. *et al.* Sea-level variability over five glacial cycles. *Nat. Commun.* **5**, 1–9
474 (2014).
- 475 35. Dutton, A., Webster, J. M., Zwartz, D. & Lambeck, K. Tropical tales of polar ice:
476 evidence of Last Interglacial polar ice sheet retreat recorded by fossil reefs of the granitic
477 Seychelles islands. *Quat. Sci. Rev.* **107**, 182–196 (2015).
- 478 36. Shackleton, S. *et al.* Is the Noble Gas-Based Rate of Ocean Warming During the Younger
479 Dryas Overestimated? *Geophys. Res. Lett.* **46**, (2019).
- 480 37. Marcott, S. A. *et al.* Centennial-scale changes in the global carbon cycle during the last
481 deglaciation. *Nature* **514**, 616–619 (2014).
- 482 38. Buizert, C. *et al.* Precise inter-polar phasing of abrupt climate change during the last ice
483 age. *Nature* **520**, 661–665 (2015).
- 484 39. Buizert, C. *et al.* The WAIS-Divide deep ice core WD2014 chronology – Part 1: Methane
485 synchronization (68 – 31 ka BP) and the gas age-ice age difference. *Clim. Past* **11**, 153
486 (2015).
- 487 40. Dykoski, C. A. *et al.* A high-resolution, absolute-dated Holocene and deglacial Asian
488 monsoon record from Dongge Cave, China. *Earth Planet. Sci. Lett.* **233**, 71–86 (2005).
- 489 41. Wang, Y. *et al.* A high-resolution absolute-dated late pleistocene monsoon record from
490 Hulu Cave, China. *Science* **294**, 2345–2348 (2001).
- 491 42. Roberts, N. L., Piotrowski, A. M., McManus, J. F. & Keigwin, L. D. Synchronous
492 Deglacial Overturning and Water Mass Source Changes. *Science* **327**, 75–78 (2010).
- 493 43. Lambeck, K., Rouby, H., Purcell, A., Sun, Y. & Sambridge, M. Sea level and global ice
494 volumes from the Last Glacial Maximum to the Holocene. *Proc. Natl. Acad. Sci.* **111**,

- 495 15296–15303 (2014).
- 496 44. Carlson, A. E. Why there was not a Younger Dryas-like event during the Penultimate
497 Deglaciation. *Quat. Sci. Rev.* **27**, 882–887 (2008).
- 498 45. Anderson, R. F. *et al.* Wind-driven upwelling in the southern ocean and the deglacial rise
499 in atmospheric CO₂. *Science* **323**, 1443–1448 (2009).
- 500 46. Toggweiler, J. R., Russell, J. L. & Carson, S. R. Midlatitude westerlies, atmospheric CO₂,
501 and climate change during the ice ages. *Paleoceanography* **21**, 1–15 (2006).
- 502 47. Marcott, S. A. *et al.* Ice-shelf collapse from subsurface warming as a trigger for Heinrich
503 events. *Proc. Natl. Acad. Sci.* **108**, 13415 LP – 13419 (2011).
- 504 48. Bassis, J. N., Peterson, S. V & Cathles, L. Mac. Heinrich events triggered by ocean
505 forcing and modulated by isostatic adjustment. *Nature* **542**, 332–334 (2017).
- 506 49. Kuhlbrodt, T. & Gregory, J. M. Ocean heat uptake and its consequences for the magnitude
507 of sea level rise and climate change. *Geophys. Res. Lett.* **39**, 1–6 (2012).
- 508 50. Pollard, D. & Deconto, R. M. Contribution of Antarctica to past and future sea-level rise.
509 *Nature* **531**, 591–597 (2016).
- 510 51. Sutter, J., Gierz, P., Grosfeld, K., Thoma, M. & Lohmann, G. Ocean temperature
511 thresholds for Last Interglacial West Antarctic Ice Sheet collapse. *Geophys. Res. Lett.* **43**,
512 2675–2682 (2016).
- 513 52. Elderfield, H. *et al.* Evolution of Ocean Temperature and Ice Volume Through the Mid-
514 Pleistocene Climate Transition. *Science* **337**, (2012).
- 515 53. Baggenstos, D. *et al.* Atmospheric gas records from Taylor Glacier, Antarctica, reveal
516 ancient ice with ages spanning the entire last glacial cycle. *Clim. Past* **13**, 943–958 (2017).
- 517 54. Buizert, C. *et al.* Radiometric 81Kr dating identifies 120,000-year-old ice at Taylor
518 Glacier, Antarctica. *Proc. Natl. Acad. Sci.* **111**, 6876–6881 (2014).
- 519 55. Aarons, S. M., Aciego, S. M., McConnell, J. R., Delmonte, B. & Baccolo, G. Dust
520 transport to the Taylor Glacier, Antarctica during the last interglacial. *Geophys. Res. Lett.*
521 **46**, 2261–2270 (2019).
- 522 56. Kuhl, T. W. *et al.* A new large-diameter ice-core drill: The Blue Ice Drill. *Ann. Glaciol.*
523 **55**, 1–6 (2014).
- 524 57. Bintanja, R. On the glaciological, meteorological, and climatological significance of
525 Antarctic blue ice areas. *Rev. Geophys.* **37**, 337–359 (1999).
- 526 58. Aciego, S. M., Cuffey, K. M., Kavanaugh, J. L., Morse, D. L. & Severinghaus, J. P.
527 Pleistocene ice and paleo-strain rates at Taylor Glacier, Antarctica. *Quat. Res.* **68**, 303–
528 313 (2007).
- 529 59. Kavanaugh, J. L. & Cuffey, K. M. Dynamics and mass balance of Taylor Glacier,
530 Antarctica: 2. Force balance and longitudinal coupling. *J. Geophys. Res.* **114**, (2009).
- 531 60. Petrenko, V. V, Severinghaus, J. P., Brook, E. J., Reeh, N. & Schaefer, H. Gas records
532 from the West Greenland ice margin covering the Last Glacial Termination : a horizontal
533 ice core. *Quat. Sci. Rev.* **25**, 865–875 (2006).
- 534 61. Bauska, T. K. *et al.* Carbon isotopes characterize rapid changes in atmospheric carbon
535 dioxide during the last deglaciation. *Proc. Natl. Acad. Sci.* **113**, 3465–3470 (2016).
- 536 62. Menking, J. A. *et al.* Spatial pattern of accumulation at Taylor Dome during Marine
537 Isotope Stage 4: stratigraphic constraints from Taylor Glacier. *Clim. Past* **15**, 1537–1556
538 (2019).
- 539 63. Blunier, T. *et al.* Synchronization of ice core records via atmospheric gases. *Clim. Past* **3**,
540 325–330 (2007).
- 541 64. Landais, A. *et al.* Two-phase change in CO₂, Antarctic temperature and global climate
542 during Termination II. *Nat. Geosci.* **6**, 1062–1065 (2013).
- 543 65. Veres, D. *et al.* The Antarctic ice core chronology (AICC2012): an optimized for the last
544 120 thousand years. *Clim. Past* **9**, 1733–1748 (2013).

- 545 66. Bereiter, B., Kawamura, K. & Severinghaus, J. P. New methods for measuring
546 atmospheric heavy noble gas isotope and elemental ratios in ice core samples. *Rapid*
547 *Commun. Mass Spectrom.* **32**, 801–814 (2018).
- 548 67. Severinghaus, J. P., Grachev, A., Luz, B. & Caillon, N. A method for precise
549 measurement of argon 40/36 and krypton/argon ratios in trapped air in polar ice with
550 applications to past firm thickness and abrupt climate change in Greenland and at Siple
551 Dome, Antarctica. *Geochim. Cosmochim. Acta* **67**, 325–343 (2003).
- 552 68. Severinghaus, J. P. & Battle, M. O. Fractionation of gases in polar ice during bubble
553 close-off: New constraints from firm air Ne, Kr and Xe observations. *Earth Planet. Sci.*
554 *Lett.* **244**, 474–500 (2006).
- 555 69. Schwander, J., Stauffer, B. & Sigg, A. Air mixing in firm and the age of the air at pore
556 close-off. *Ann. Glaciol.* **10**, 141–145 (1988).
- 557 70. Schwander, J. The transformation of snow to ice and the occlusion of gases. in *The*
558 *Environmental Record in Glaciers and Ice Sheets* (eds. Oeschger, H. & Langway, C. C.)
559 53–67 (1989).
- 560 71. Severinghaus, J. P., Sowers, T., Brook, E. J., Alley, R. B. & Bender, M. L. Timing of
561 abrupt climate change at the end of the younger dryas interval from thermally fractionated
562 gases in polar ice. *Nature* **391**, 141–146 (1998).
- 563 72. Hamme, R. C. & Severinghaus, J. P. Trace gas disequilibria during deep-water formation.
564 *Deep Sea Res.* **54**, 939–950 (2007).
- 565 73. Nilsson, J. *et al.* Ice-shelf damming in the glacial Arctic Ocean: dynamical regimes of a
566 basin-covering kilometre-thick ice shelf. *Cryosph.* **11**, 1745–1765 (2017).
- 567 74. Kolmogorov, A. N. *Foundations of the Theory of Probability*. (Chelsea Publishing
568 Company, 1950).

569
570 **Corresponding Author**

571 Correspondence and request for materials should be addressed to S.S. at sshackle@ucsd.edu.

572

573 **Acknowledgements**

574

575 This research was supported by NSF grants 1246148 (SIO), 1245821 (OSU) and 1245659 (UR).
576 We thank Kathy Schroeder, Mike Jayred, Peter Sperlich, Isaac Vimont, Jacob Ward, Heidi Roop,
577 Peter Neff, and Andrew Smith for their invaluable field support for this project. Ice Drilling Design
578 and Operations (IDDO) provided drilling support, and the US Antarctic Program provided
579 logistical support for this project. Thanks to Ross Beaudette for lab support at SIO, to Michael Kalk
580 for CO₂ measurements at OSU, and to Monica Arienzo and Nathan Chellman for their heroic
581 operation of the continuous melting system at DRI. The research at University of Bern leading to
582 these results has received funding from the European Research Council (ERC) under the European
583 Union's Seventh Framework Programme FP7/2007-2013 ERC Grant 226172 (ERC Advanced
584 Grant Modern Approaches to Temperature Reconstructions in polar Ice Cores (MATRICs)) and
585 the Swiss national Science Foundation (200020_172506 (iCEP), 200021_155906 (NOTICE)). The
586 EDC samples were obtained under the framework of EPICA, a joint European Science
587 Foundation/European Commission scientific program funded by the European Union and national
588 contributions from Belgium, Denmark, France, Germany, Italy, the Netherlands, Norway, Sweden,
589 Switzerland, and the United Kingdom. The main logistic support was provided by IPEV and PNRA
590 at Dome C.

591

592 **Author Contributions**

593

594 J.P.S. and S.S. designed research. S.S., M.H., D.B., and T.K. performed noble gas measurements.
595 J.A.M., E.J.B., R.H.R., J.R.M. and S.S. performed trace gas field/lab measurements for Taylor
596 Glacier age model. S.S., D.B., J.A.M., M.N.D., B.B., T.K.B., R.H.R, E.J.B., V.V.P., M.J.R., T.K.,
597 M.H., J.S., H.F., and J.P.S. analyzed data. S.S. wrote the paper with input from all authors.
598